Temperature dependence of the repulsive core potential in heavy-ion fusion reactions

O. N. Ghodsi* and R. Gharaei
Sciences Faculty, Department of Physics, University of Mazandaran, P.O. Box 47415-416, Babolsar, Iran
(Received 15 April 2012; revised manuscript received 11 June 2012; published 26 June 2012)

In this work, we expand upon our previous study, the effect of hot nuclear matter on the calculation of the internuclear potential [Phys. Rev. C **84**, 024612 (2011)], to the ^{28}Si + ^{40}Ca, ^{35}Cl + ^{48}Ti, and ^{40}Ar + ^{74}Ge collision systems. For this purpose, we have employed the equation of state of hot nuclear matter, which is based on density-dependent Seyler-Blanchard formalism at finite temperature, to discuss the energy dependence of a repulsive core potential in the nucleon-nucleon interaction. The obtained values for strength of this potential show a linear dependence as a function of excitation energy E^* (or temperature T) of the compound nucleus. Indeed, it is predictable that the effect of hot nuclear matter on heavy-ion reactions can be formulated by an additional energy-dependent function in the nucleon-nucleon potential.

DOI: 10.1103/PhysRevC.85.064620 PACS number(s): 25.70.Jj, 21.65.Mn

I. INTRODUCTION

The effect of nuclear matter incompressibility on the heavy-ion fusion process has always been one of the interesting subjects which is attracted much attention in recent years [1–9]. It has been shown that some observed discrepancies between theoretical and experimental fusion cross section data can be explained by this effect. Some of these recent investigations are presented in the following

Jiang and collaborators identified an unexpected behavior of fusion data for heavy- and medium-mass collision systems at deep sub-barrier energies [10]. They demonstrated that the experimental fusion cross section data in comparison with the theoretical cross sections, which are based on the coupled-channels (CC) calculations, are suddenly suppressed at these energy ranges. In another theoretical study it was suggested that the fusion hindrance, which prevents the overlapping of the wave functions of two systems of fermions, can explain this unexpected phenomenon [8] and one can simulate it by an additional repulsive force in the nucleon-nucleon (NN) interaction [8,11]. It is illustrated that the implementation of this corrective effect on an M3Y-type NN interaction (M3Y + repulsion) can reproduce the fusion cross section data with high accuracy. This modification also exhibits a shallow pocket in the inner regions of the Coulomb barrier.

In another study, it is shown that the anomalous increase of the diffuseness parameter of the Woods-Saxon (WS) potential in fusion reactions [12–16] could be due to the effect of the fusion hindrance on the calculation of the internuclear potential [7]. Investigations performed on the fusion reactions of ^{12}C, ^{16}O, ^{28}Si, and ^{35}Cl with ^{92}Zr reveal that accounting for the effect of the nuclear matter equation of state (EOS) in the calculation of the internuclear potential can explain the increase of the diffuseness parameter up to 0.73 fm.

The corrective effect of the nuclear matter EOS has been even used for light-ion fusion reactions. By using the M3Y + repulsion potential accompanied by CC calculations, the effect of the mutual excitations on the fusion cross sections have been examined for ^{12}C + ^{12}C, ^{12}C + ^{13}C, and ^{13}C + ^{13}C isotopic systems [5]. The results obtained reveal that this effect has an important role in calculation of fusion cross sections for reactions with carbon isotopes.

In previous work, we have considered the thermal effects of a compound nucleus in the modeling of a repulsive core [6]. For this purpose, the EOS of hot nuclear matter (HNM) is employed to compute the energy per particle of finite nuclear matter within the complete overlapping region of density distributions of colliding nuclei. The investigation, which was performed on the ^{40}Ar + ^{40}Ca system, indicated that the temperature of the compound nucleus plays an important role in the predictions of fusion data. In the present study, we shall expand upon our investigations of these effects to three other systems, namely, ^{28}Si + ^{40}Ca, ^{35}Cl + ^{48}Ti, and ^{40}Ar + ^{74}Ge.

Section II introduces the theoretical formalism which is employed to calculate the nuclear potential. A description of the thermal conditions for the considered reactions is given in Sec. III. In Sec. IV, we describe the employed procedure for calculating fusion cross sections. Section V is devoted to some concluding remarks.

II. CALCULATION OF the NUCLEAR POTENTIAL

During the last four decades, many theoretical models have been introduced to calculate the heavy-ion interaction potential. The Skyrme energy density formalism [17], proximity potentials [18], and double folding (DF) model [19,20] are examples of these models. In the first model, the difference between the energy expectation value E of the interacting system at finite separation distance $r = R$ and infinity, $r = \infty$, is defined as the interaction potential:

$$V(R) = E(R) - E(\infty), \tag{1}$$

where the energy expectation value E of a nucleus can be expressed as the integral of the energy density functional [17],

$$E = \int H(\mathbf{r})\, d\mathbf{r}, \tag{2}$$

*o.nghodsi@umz.ac.ir

where $H(\mathbf{r})$ is the energy density function. So far different aspects of heavy-ion reactions have studied using this formalism [21–24].

When two surfaces approach each other within a distance of 2–3 fm, an additional force due to the proximity of the surfaces will appear; this is called the proximity potential. All versions of this model are based on the proximity force theorem [18]. According to this theory, the nuclear potential is defined as the product of a geometrical factor and a universal function, which are, respectively, dependent on the mean curvature of the interaction surface and the separation distance. Furthermore, this model is independent of the masses of colliding nuclei. Different versions of the proximity model have been introduced in Refs. [18,25–28]

To calculate the nucleus-nucleus potential, we have used the DF model [19,20]. In this model, the nuclear potential between two colliding nuclei can be calculated by

$$V_{\mathrm{DF}}(\mathbf{R}) = \int d\mathbf{r}_1 \int d\mathbf{r}_2\, \rho_1(\mathbf{r}_1)\rho_2(\mathbf{r}_2)\upsilon_{\mathrm{NN}}(\mathbf{r}_{12} = \mathbf{R} + \mathbf{r}_2 - \mathbf{r}_1), \tag{3}$$

where υ_{NN} is the NN interaction. In this calculation, we have used the M3Y-Paris [29] effective interaction with a zero-range approximation for its exchange part. One of the main inputs in the DF model is the density distribution, $\rho_i(r_i)$, of the interacting nuclei. Here, we have used a two-parameter Fermi-Dirac (2PF) distribution function,

$$\rho_{2\mathrm{PF}}(r) = \frac{\rho_0}{1 + \exp\left[(r - R_0)/a_0\right]}, \tag{4}$$

and a three-parameter Fermi-Dirac (3PF) distribution function,

$$\rho_{3\mathrm{PF}}(r) = \frac{\rho_0(1 + \omega r^2/R_0^2)}{1 + \exp\left[(r - R_0)/a_0\right]}, \tag{5}$$

for parametrization of the density in the participant nuclei. For ^{28}Si, ^{40}Ar, and ^{48}Ti nuclei, we have used the 2PF profile whereas the nuclear distribution density in ^{35}Cl and ^{40}Ca is parametrized based on the 3PF profile. The parameters of these profiles are evaluated experimentally [30]. For the ^{74}Ge nucleus, we have used the Hartree-Fock-Bogoliubov (HFB) calculations [31]. The values of R_0, a_0, and ω parameters based on the 2PF and 3PF profiles for selected nuclei are listed in Table I. Additional details of the calculation of the DF model are presented in Ref. [32].

It is well known that the DF formalism is based on the sudden approximation. Indeed, the density distribution of interacting nuclei is assumed to be frozen during the fusion process. This causes the density of nuclear matter in the overlapping region to increase to twice the saturation density of nuclear matter, namely, 0.16 fm^{-3}. This unusual physical effect can be modified by adding a repulsive core term to the nuclear attractive potential in the DF calculation. As noted in Sec. I, one can employ the proposed procedure in Ref. [8] to calculate this corrective term. The strength of the repulsive core potential is defined by

$$V_{\mathrm{rep}}(\mathbf{R} = 0) = \nu_{\mathrm{rep}} \int d\mathbf{r}_1 \int d\mathbf{r}_2\, \delta(\mathbf{r}_2 - \mathbf{r}_1)\rho_1(\mathbf{r}_1)\rho_2(\mathbf{r}_2), \tag{6}$$

where its central part is parametrized by a zero-range interaction and it is evaluated within the complete overlapping region of density distributions. We should point out that when considering surface diffuseness effects of interacting nuclei during overlapping of density distributions, the diffuseness parameters of the target and the projectile in Eqs. (4) and (5) are defined as $a_0 = a_{\mathrm{rep}}$. Therefore, we consider two adjustable parameters, a_{rep} and ν_{rep}, for calculating the repulsive core potential.

When two interacting nuclei approach each other, the overlapping of their density distributions begins at a distance of $R < R_1 + R_2$, where R_1 and R_2 are the nuclear radii of target and projectile, respectively. Because the energy per nucleon of finite nuclear matter is directly dependent on density, it is predictable that increasing the density in the overlapping region enhances the energy of the system. This increase of energy can be formulated for cold nuclear matter as the difference between the initial $E(\rho \approx \rho_0)$ and final $E(\rho \approx 2\rho_0)$ states,

$$\Delta U|_{T=0} \approx 2A_P[E(2\rho_o) - E(\rho_o)], \tag{7}$$

where ρ_o is the saturation density of nuclear matter. In this formalism, the number of nucleons in the overlapping region of an asymmetric system is considered twice those in the smaller nucleus, A_P.

TABLE I. The parameters of density distribution for different nuclei. The parameters of 2PF and 3PF profiles are taken from Refs. [30,31].

Nucleus	Profile	R_0 (fm)	a_0 (fm)	ω
^{28}Si	2PF	3.14(6)	0.537(32)	
^{35}Cl	3PF	3.476(32)	0.559(5)	−0.10(2)
^{40}Ar	2PF	3.53(4)	0.542(15)	
^{40}Ca	3PF	3.766(23)	0.586(5)	−0.161(23)
^{48}Ti	2PF	3.843(15)	0.588(5)	
^{74}Ge	2PF	4.5631	0.5184	

III. DESCRIPTION OF THE THERMAL CONDITIONS OF THE FUSION PROCESS

By eliminating thermal effects of the compound nucleus during the fusion process, one can use the cold nuclear matter EOS based on the Thomas-Fermi (TF) model [33] for calculating the energy per nucleon, $E(\rho)$, in Eq. (7). In fusion reactions with $T \geqslant 2$ MeV, the EOS predicted by theoretical models such as TF may be unsuitable owing to the disappearance of shell effects. Therefore, we have employed the hot EOS, which has been generalized using the modified density-dependent terms in the Seyler-Blanchard (SB) formalism [34], to compute the energy per nucleon of HNM. In recent years, the hot EOS has been used for various studies such as calculation of the hot G-matrix using an extension of the Pauli operator [35], collective flow and multifragmentation [36], and entropy production and thermalization in medium-energy heavy-ion collisions [37].

TABLE II. The parameters of the WS potential for considered reactions which are determined by fitting to the M3Y + repulsion potential at each bombarding energy (or temperature T). The χ^2 vales are the corresponding relative errors.

Reaction	$E_{\text{c.m.}}$ (MeV)	T (MeV)	V_0	r_0	a	χ^2
$^{28}\text{Si} + ^{40}\text{Ca}$	175.2	4.85	71.6	1.16	0.719	$6.801(65) \times 10^{-8}$
	181.7	4.94	71.4	1.16	0.722	$5.883(07) \times 10^{-8}$
	192.3	5.08	66.9	1.17	0.721	$5.462(98) \times 10^{-8}$
	233.5	5.60	73.0	1.16	0.723	$5.948(36) \times 10^{-8}$
	265.8	5.97	64.5	1.77	0.719	$5.396(47) \times 10^{-8}$
$^{35}\text{Cl} + ^{48}\text{Ti}$	57.5	2.43	31.9	1.25	0.759	$9.462(96) \times 10^{-10}$
	69.1	2.68	38.5	1.25	0.754	$1.124(19) \times 10^{-9}$
	80.6	2.91	56.5	1.20	0.745	$1.113(34) \times 10^{-9}$
	92.2	3.12	59.3	1.19	0.738	$1.125(33) \times 10^{-9}$
$^{40}\text{Ar} + ^{74}\text{Ge}$	108.4	2.71	53.2	1.18	0.718	$1.105(06) \times 10^{-8}$
	127.8	2.98	59.4	1.18	0.717	$1.014(97) \times 10^{-8}$
	147.3	3.23	63.8	1.17	0.717	$1.181(33) \times 10^{-8}$

By implementing thermal effects of the compound nucleus, the increasing energy of the system based on Eq. (7) can be modified as

$$\Delta U(T) \approx 2A_P[E_H(2\rho_o, T) - E_C(\rho_o)], \tag{8}$$

where the subscripts H and C, respectively, refer to the hot and the cold nuclear matter. In order to calculate $E_H(\rho, T)$, we have used the following relation [34]:

$$E_H(\rho, T) = E_0(\rho, T = 0) + E_T(\rho, T), \tag{9}$$

where $E_0(\rho, T = 0)$ and $E_T(\rho, T)$ are the energy per nucleon of nuclear matter at zero ($T = 0$) and finite (T) temperatures, which are introduced in Ref. [34]. T is related to the excitation energy E^* of the compound nucleus or the energy of the projectile nucleus in the center-of-mass frame, $E_{\text{c.m.}}$, via the entrance channel Q_{in} value, as

$$E^* = E_{\text{c.m.}} + Q_{\text{in}} = \frac{1}{a}AT^2 - T, \tag{10}$$

with $a = 9$ or 10 for intermediate-mass or superheavy systems, respectively [38,39]. Using this equation, we have computed the corresponding values of compound nucleus temperature for each considered reaction, namely, $^{28}\text{Si} + ^{40}\text{Ca}$, $^{35}\text{Cl} + ^{48}\text{Ti}$, and $^{40}\text{Ar} + ^{74}\text{Ge}$; these are listed in Table II.

One can see that the temperature of the compound nucleus for some systems increases to values of about 6 MeV. This can be attributed to the high excitation energies of the compound nucleus. Note that all selected reactions are medium-mass systems with negative Q values.

In order to obtain the parameters of the repulsive core modeling, we have used the following relation:

$$\Delta U(T) = V_{\text{NN}}(0) = V_{\text{atr}}(0) + V_{\text{rep}}(0). \tag{11}$$

In this relation the nucleus-nucleus potential $V_{\text{NN}}(R)$ is defined as the sum of attractive, $V_{\text{atr}}(R)$, and repulsive, $V_{\text{rep}}(R)$, parts, which are estimated within complete overlapping region of density distributions, $R = 0$. To compute the last term, one should minimize the chi-squared value (χ^2) for fusion cross sections σ_{fus} at each energy by adjusting the repulsive parameters a_{rep} and ν_{rep}. The theoretical approach for calculating the values of σ_{fus} is described in Sec. IV.

The calculated total potentials based on the M3Y and M3Y + repulsion models at specified bombarding energy are shown in Fig. 1. The influence of the repulsive core potential on the inner regions of the Coulomb barrier is quite evident. This extra repulsive force increases the barrier thickness and exhibits a shallow pocket in the $R < R_B$ region. As a result of Fig. 1, one can find out that the M3Y potential is an unphysical form of interaction potential in the inner regions of the Coulomb barrier, because it is much deeper than the ground-state energy of the compound nucleus.

Now let us study the temperature dependence of the two introduced quantities ΔU and V_{rep} for $^{28}\text{Si} + ^{40}\text{Ca}$, $^{35}\text{Cl} + ^{48}\text{Ti}$, and $^{40}\text{Ar} + ^{74}\text{Ge}$ fusion reactions. By using Eq. (8), the trend of variations $\Delta U(T)$ at each temperature T can be analyzed. In Fig. 2, the variations of $\Delta U(T)$ versus the bombarding energy in the center-of-mass frame for the chosen systems are shown. It can be seen that the values of $\Delta U(T)$ increase with increasing energy (or temperature T). Moreover, these trends show a linear dependence on T.

For each set of selected parameters of a_{rep} and ν_{rep}, we have calculated the values of V_{rep} at $R = 0$ using Eq. (6), and these results are illustrated in Fig. 3. The obtained results show that there is a linear dependence between the strength of the repulsive core and the bombarding energy or temperature of the compound nucleus.

IV. CALCULATION OF FUSION CROSS SECTIONS

We have analyzed the fusion cross sections for the chosen systems $^{28}\text{Si} + ^{40}\text{Ca}$, $^{35}\text{Cl} + ^{48}\text{Ti}$, and $^{40}\text{Ar} + ^{74}\text{Ge}$, [40–42], using the CCFULL code [43]. In general, the coupling between the relative motions and the intrinsic degrees of freedom of the interacting nuclei plays an important role in the analytical calculations of fusion cross sections. The CCFULL code takes into account the effects of nonlinear couplings to full order. On the other hand, in this code, the nuclear interaction potential has been assumed to be in WS form. The obtained results for WS parameters, which have been achieved from the fitting to the M3Y + repulsion potentials at each bombarding energy, are listed in Table II. The corresponding values of the relative

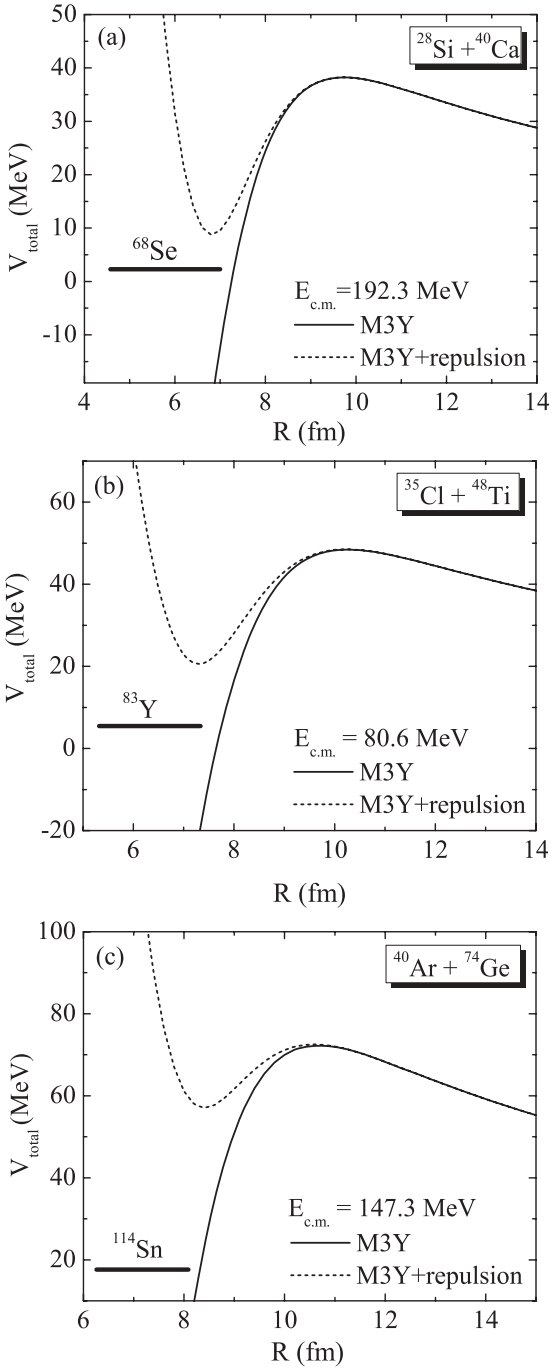

FIG. 1. Comparison of total interaction potentials based on the M3Y and M3Y + repulsion models for reactions of (a) ^{28}Si + ^{40}Ca, (b) ^{35}Cl + ^{48}Ti, and (c) ^{40}Ar + ^{74}Ge. In each panel, the values of the energy for which the M3Y + repulsion potential has been calculated and the ground-state energies of the compound nuclei for each reaction are also shown.

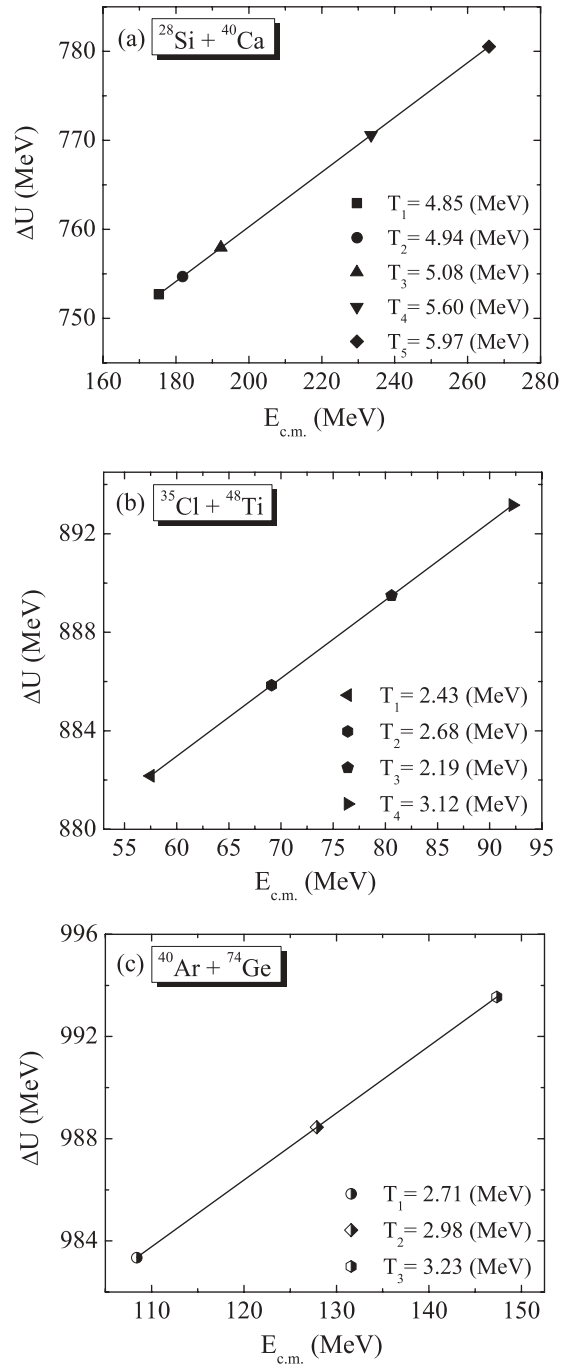

FIG. 2. The values of ΔU at different bombarding energy, calculated by Eq. (8) for (a) ^{28}Si + ^{40}Ca, (b) ^{35}Cl + ^{48}Ti, and (c) ^{40}Ar + ^{74}Ge fusion reactions. In each panel, the corresponding temperature values of the compound nucleus, T (in MeV), have also been displayed.

errors of fitting, χ^2, have also been reported in this table. It is quite evident that the parameters of the WS potential are obtained with high accuracy. In the present work, the coupled channels calculations are based on the low-lying excited states 2^+ and 3^- in the participant nuclei. The nuclear structure inputs of these states for ^{40}Ar, ^{40}Ca, ^{48}Ti, and ^{74}Ge nuclei are given in Table III. For excited states of ^{28}Si and ^{35}Cl, we have used phonon states reported in Ref. [12]. Therefore, we have employed the phonon states 2^+ with $\beta_2^N = 0.25$ for ^{28}Si and 3^- with $\beta_2^N = 0.252$ and excitation energy $E^* = 1.763$ MeV for ^{35}Cl. The calculated values of fusion cross sections based on the M3Y + repulsion potential corresponding to each bombarding energy, $E_{c.m.}$, are listed in

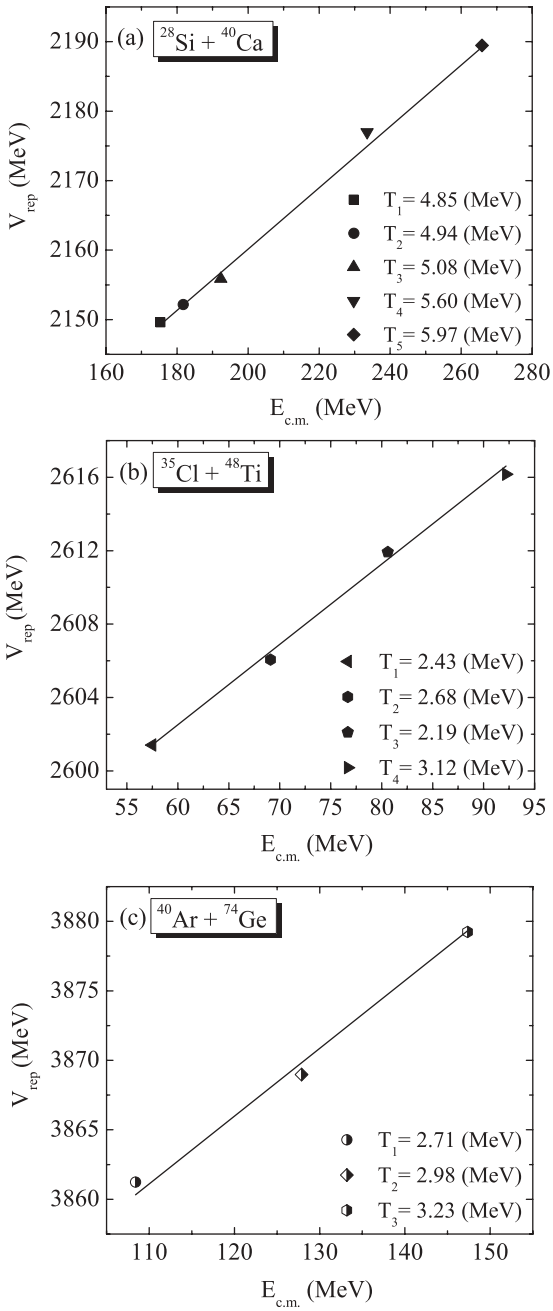

FIG. 3. Repulsive core strength V_{rep} (in MeV) as a function of $E_{c.m.}$ for (a) ^{28}Si + ^{40}Ca, (b) ^{35}Cl + ^{48}Ti, and (c) ^{40}Ar + ^{74}Ge fusion reactions. In each panel, the corresponding temperature values T (in MeV) are also shown. The solid lines have been drown to represent the linear dependence of V_{rep} values.

Table IV. In this table, the experimental fusion cross section data are also listed for selected reactions.

To achieve further understanding, we have compared our obtained results for the interaction potential and fusion cross section with some proximity potentials, namely, AW 95 [44], Bass 80 [45], and Prox. 2010 [26]. In recent years, these potentials have been applied to more than 400 fusion reactions and compared with experimental data [26–28]. The obtained results of these studies show that among various versions of proximity potentials, the AW 95, Bass 80, and Prox. 2010 potentials have the best agreement with experimental data (for instance, see Fig. 3 of both Refs. [26,28]).

TABLE III. The values of the excitation energies E^*, reduced transition probabilities $B(E\lambda)$, and corresponding deformation parameters β_λ of low-lying 2^+ and 3^- states for chosen nuclei. These values are extracted from Refs. [48,49].

Nucleus	λ^π	E^* (MeV)	$B(E\lambda)$ (e^2 b$^\lambda$)	β_λ
^{40}Ar	2^+	1.460	0.0330	0.251
	3^-	3.681	0.0087	0.314
^{40}Ca	2^+	3.904	0.0099	0.123
	3^-	3.737	0.0204	0.432
^{48}Ti	2^+	0.983	0.0720	0.269
	3^-	3.359	0.0067	0.197
^{74}Ge	2^+	0.596	0.3000	0.282
	3^-	2.536	0.0200	0.145

The original proximity formalism, i.e., Prox. 77 [18], has been generalized by using the thermal effects of the compound nucleus [46,47]. In the proposed formalism, the effective sharp radius R_{0i} and the nuclear surface thickness b are modified as $R_{0i}(T) = R_{0i}(T = 0)(1 + 0.0007T^2)$ and $b(T) = 0.99(1 + 0.009T^2)$, respectively. In the present study, we have applied temperature effects of the compound nucleus on the selected proximity potentials. In Fig. 4, we have compared the temperature-dependent potentials, which are based on the M3Y + repulsion and various versions of proximity models, at specified energy for fusion systems of ^{28}Si + ^{40}Ca, ^{35}Cl + ^{48}Ti, and ^{40}Ar + ^{74}Ge. This figure shows that the shallow pockets caused by the Prox. 2010 potential are deeper than in other models.

The percentage difference between theoretical and experimental fusion cross sections,

$$\Delta\sigma_{fus}(\%) = \left(\frac{\sigma_{theor} - \sigma_{exp}}{\sigma_{exp}}\right) \times 100, \qquad (12)$$

TABLE IV. The calculated results of fusion cross sections σ_{theor} based on the M3Y + repulsion potential for selected reactions ^{28}Si + ^{40}Ca, ^{35}Cl + ^{48}Ti, and ^{40}Ar + ^{74}Ge. In this table, the experimental fusion cross sections σ_{exp} and their corresponding errors $\pm\delta\sigma$ are also listed [40–42].

Reaction	$E_{c.m.}$ (MeV)	σ_{theor} (mb)	$\sigma_{exp} \pm \delta\sigma$ (mb)
^{28}Si + ^{40}Ca	175.2	658.4	646 ± 100
	181.7	635.4	631 ± 126
	192.3	556.5	548 ± 130
	233.5	512.8	519 ± 104
	265.8	372.4	379 ± 76
^{35}Cl + ^{48}Ti	57.5	337.3	324 ± 17
	69.1	667.4	668 ± 33
	80.6	947.3	948 ± 47
	92.2	1121.2	1140 ± 106
^{40}Ar + ^{74}Ge	108.4	832.5	830 ± 80
	127.8	931.3	930 ± 100
	147.3	906.5	910 ± 100

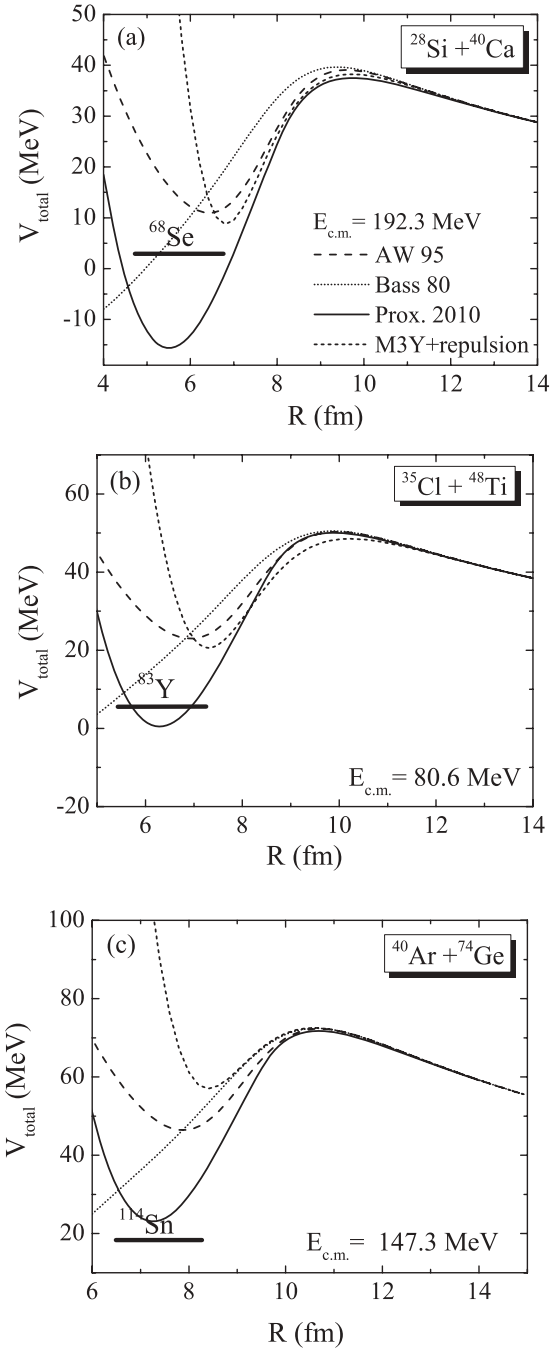

FIG. 4. Comparison of temperature-dependent potentials based on the M3Y + repulsion, AW 95, Bass 80, and Prox. 2010 models for (a) ^{28}Si + ^{40}Ca (at $E_{c.m.} = 192.3$ MeV), (b) ^{35}Cl + ^{48}Ti (at $E_{c.m.} = 80.6$ MeV), and (c) ^{40}Ar + ^{74}Ge (at $E_{c.m.} = 147.3$ MeV) fusion reactions.

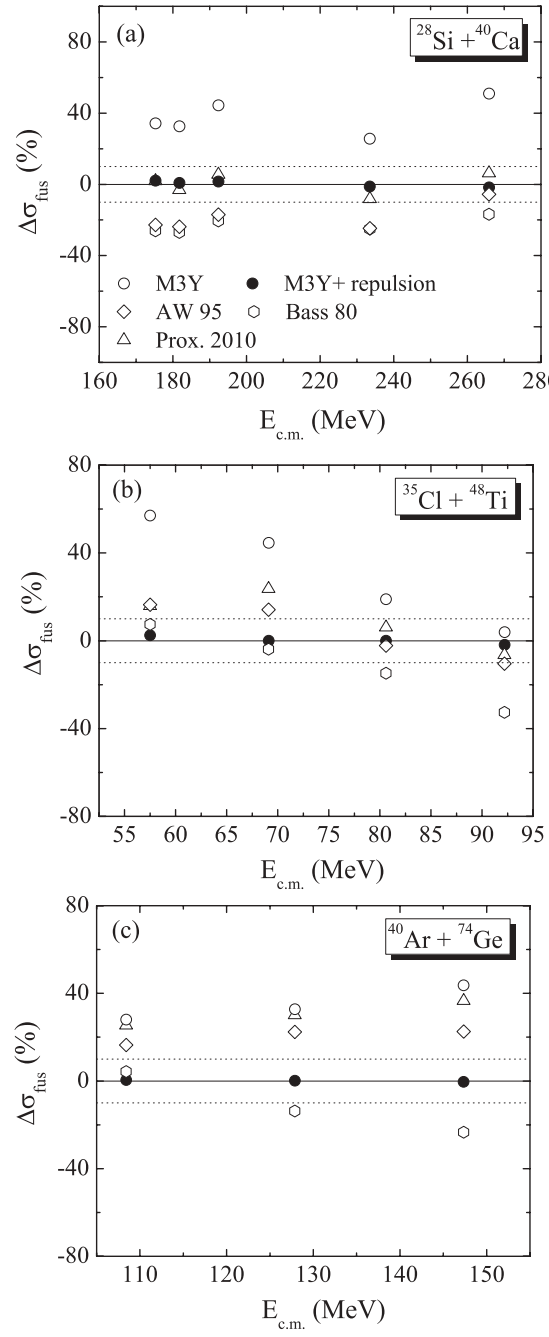

FIG. 5. Ratio of the measured [40–42] and calculated values of the fusion cross section resulting from M3Y, M3Y + repulsion, AW 95, Bass 80, and Prox. 2010 potentials for reactions of (a) ^{28}Si + ^{40}Ca, (b) ^{35}Cl + ^{48}Ti, and (c) ^{40}Ar + ^{74}Ge.

for ^{28}Si + ^{40}Ca, ^{35}Cl + ^{48}Ti, and ^{40}Ar + ^{74}Ge collision systems has been illustrated in Fig. 5. One can see that our calculated fusion cross sections are consistent with those evaluated experimentally. In this figure, the predictions of selected proximity potentials for Eq. (12) are also shown. It is clear that the results which are obtained by the Prox. 2010 potential in comparison to the other proximity models are in better agreement with empirical fusion cross section data.

V. CONCLUSIONS

In this study, we have analyzed the thermal effects of a compound nucleus on the entrance channel potentials and fusion excitation functions for reactions of ^{28}Si + ^{40}Ca, ^{35}Cl + ^{48}Ti, and ^{40}Ar + ^{74}Ge. To calculate the interaction potential and fusion cross sections the modified DF model and CC formalism are employed, respectively. The obtained results of the present work can be calibrated to the following cases:

(i) It is indicated that the thermal effects of a compound nucleus play a significant role in the calculation of the nuclear potential and the cross section. Furthermore, this effect considerably improves the agreement between calculated and measured fusion cross section data (see Fig. 5).

(ii) The values of the repulsive core strength within complete overlapping region of density distributions ($R = 0$) increase with increasing bombarding energy. The analysis of the $^{28}\mathrm{Si} + {}^{40}\mathrm{Ca}$, $^{35}\mathrm{Cl} + {}^{48}\mathrm{Ti}$, and $^{40}\mathrm{Ar} + {}^{74}\mathrm{Ge}$ systems reveals that this behavior is true for all of these selected reactions.

(iii) The obtained results show that the repulsive core potential V_{rep} at $R = 0$ has a linear dependence as a function of the energy (or temperature T) of the compound nucleus for fusion reactions with a thermal condition of $T \geqslant 2$ MeV.

(iv) In this study, we have compared the predictions of temperature-dependent models for interaction potentials and fusion cross sections (see Figs. 4 and 5). At our selected energy ranges, it is shown that the M3Y + repulsion potential can explain the experimental fusion cross sections within $\pm 3\%$, on average. This relative error is smaller than the obtained values from other considered models, namely, M3Y double folding and proximity potentials.

(v) Using the obtained thermal predictions for the interaction potentials and fusion cross sections based on the proximity models, one can estimate that more research is needed for the proposed form of $R_{0i}(T)$ and $b(T)$ at our selected energy ranges.

(vi) The modeling of thermal effects of the compound nucleus using the suggested form $\upsilon_{\mathrm{rep}}(\mathbf{r}, E)$ may be an interesting subject to study in further work.

[1] G. Montagnoli *et al.*, Phys. Rev. C **85**, 024607 (2012).
[2] V. Zanganeh, N. Wang, and O. N. Ghodsi, Phys. Rev. C **85**, 034601 (2012).
[3] S. Misicu and F. Carstoiu, Phys. Rev. C **83**, 054622 (2011).
[4] S. Misicu and F. Carstoiu, Phys. Rev. C **84**, 051601(R) (2011).
[5] H. Esbensen, X. Tang, and C. L. Jiang, Phys. Rev. C **84**, 064613 (2011).
[6] O. N. Ghodsi and R. Gharaei, Phys. Rev. C **84**, 024612 (2011).
[7] O. N. Ghodsi and V. Zanganeh, Nucl. Phys. A **846**, 40 (2010).
[8] S. Misicu and H. Esbensen, Phys. Rev. C **75**, 034606 (2007).
[9] C. L. Jiang *et al.*, Phys. Lett. B **640**, 18 (2006).
[10] C. L. Jiang *et al.*, Phys. Rev. Lett. **89**, 052701 (2002).
[11] E. Uegaki, and Y. Abe, Prog. Theor. Phys. **90**, 615 (1993).
[12] J. O. Newton, C. R. Morton, M. Dasgupta, J. R. Leigh, J. C. Mein, D. J. Hinde, H. Timmers, and K. Hagino, Phys. Rev. C **64**, 064608 (2001).
[13] I. I. Gontchar, D. J. Hinde, M. Dasgupta, and J. O. Newton, Nucl. Phys. A **722**, C479 (2003).
[14] J. O. Newton, R. D. Butt, M. Dasgupta, D. J. Hinde, I. I. Gontchar, C. R. Morton, and K. Hagino, Phys. Rev. C **70**, 024605 (2004).
[15] A. Mukherjee, D. J. Hinde, M. Dasgupta, K. Hagino, J. O. Newton, and R. D. Butt, Phys. Rev. C **75**, 044608 (2007).
[16] K. Hagino, T. Takehi, A. B. Balantekin, and N. Takigawa, Phys. Rev. C **71**, 044612 (2005).
[17] D. Vautherin and D. M. Brink, Phys. Rev. C **5**, 626 (1972).
[18] J. Blocki, J. Randrup, W. J. Swiatecki, and C. F. Tsang, Ann. Phys. (NY) **105**, 427 (1977).
[19] G. R. Satchler and W. G. Love, Phys. Rep. **55**, 183 (1979).
[20] D. T. Khoa and G. R. Satchler, Nucl. Phys. A **668**, 3 (2000).
[21] R. K. Puri, P. Chattopadhyay, and R. K. Gupta, Phys. Rev. C **43**, 315 (1991).
[22] R. K. Puri and R. K. Gupta, Phys. Rev. C **45**, 1837 (1992).
[23] Q.-B. Shen, Y.-L. Han, and H.-R. Guo, Phys. Rev. C **80**, 024604 (2009).
[24] M. Liu, N. Wang, Z. Li, X. Wu, and E. Zhao, Nucl. Phys. A **768**, 80 (2006).
[25] W. D. Myers, and W. J. Swiatecki, Phys. Rev. C **62**, 044610 (2000).
[26] I. Dutt and R. K. Puri, Phys. Rev. C **81**, 047601 (2010).
[27] I. Dutt and R. K. Puri, Phys. Rev. C **81**, 044615 (2010).
[28] I. Dutt and R. K. Puri, Phys. Rev. C **81**, 064609 (2010).
[29] G. Bertsch, J. Borysowicz, H. McManus, and W. G. Love, Nucl. Phys. A **284**, 399 (1977).
[30] H. de Vries, C. W. deJager, and C. de Vries, At. Data Nucl. Data Tables **36**, 495 (1987).
[31] [http://www-nds.iaea.org/RIPL-2/masses.html].
[32] O. N. Ghodsi, M. Mahmoodi, and J. Ariai, Phys. Rev. C **75**, 034605 (2007).
[33] W. D. Myers and W. J. Swiatecki, Act. Phys. Pol. B **26**, 111 (1995).
[34] H. M. M. Mansour and Kh. A. Ramadan, Phys. Rev. C **57**, 1744 (1998).
[35] R. K. Puri, N. Ohtsuka, E. Lehmann, Amand Faessler, M. A. Matin, Dao T. Khoa, G. Batko, and S. W. Huang, Nucl. Phys. A **575**, 733 (1994).
[36] Y. K. Vermani, S. Goyal, and R. K. Puri, Phys. Rev. C **79**, 064613 (2009).
[37] Y. K. Vermani and R. K. Puri, Nucl. Phys. A **847**, 243 (2010).
[38] R. K. Puri and R. K. Gupta, J. Phys. G **18**, 903 (1992).
[39] R. K. Gupta, S. Singh, R. K. Puri, A. Sandulescu, w. Greiner, and W. Scheid, J. Phys. G **18**, 1533 (1992).
[40] M. F. Vineyard *et al.*, Phys. Rev. C **45**, 1784 (1992).
[41] W. Scobel, H. H. Gutbrod, M. Blann, and A. Mignerey, Phys. Rev. C **14**, 1808 (1976).
[42] H. Gauvin, D. Guerreau, Y. Le Beyec, M. Lefort, F. Plasil, and X. Tarrago, Phys. Lett. B **58**, 163 (1975).
[43] K. Hagino, N. Rowley, and A. T. Kruppa, Comput. Phys. Commun. **123**, 143 (1999).
[44] A. Winther, Nucl. Phys. A **594**, 203 (1995).
[45] R. Bass, in *Inelastic and Fusion Reactions with Heavy Ions*, edited by W. von Oertzen, Lecture Notes in Physics, Vol. 117 (Springer-Verlag, Berlin, 1980), p. 281.
[46] R. Kumar, M. Bansal, S. K. Arun, and R. K. Gupta, Phys. Rev. C **80**, 034618 (2009).
[47] R. Kumar, Phys. Rev. C **84**, 044613 (2011).
[48] S. Raman, C. W. Nestor Jr., and P. Tikkanen, At. Data Nucl. Data Tables **78**, 1 (2001).
[49] R. H. Spear, At. Data Nucl. Data Tables **42**, 55 (1989).